Cosmic ray ground level enhancements: Power of the pulse shape

Olakunle Ogunjobi

Du Toit Strauss

Harm Moraal

K.G. McCracken

R.A. Caballero-Lopez

University of KwaZulu-Natal

Durban, South Africa

NORTH-WEST UNIVERSITY
YUNIBESITI YA BOKONE-BOPHIRIMA
NOORDWES-UNIVERSITEIT

UKZN, ATM-RES, 06 OCT. 2016

UNIVERSITY OF KWAZULU-NATAL
INYUVESI YAKWAZULU-NATALI

Solar flare and coronal mass ejection - shocks

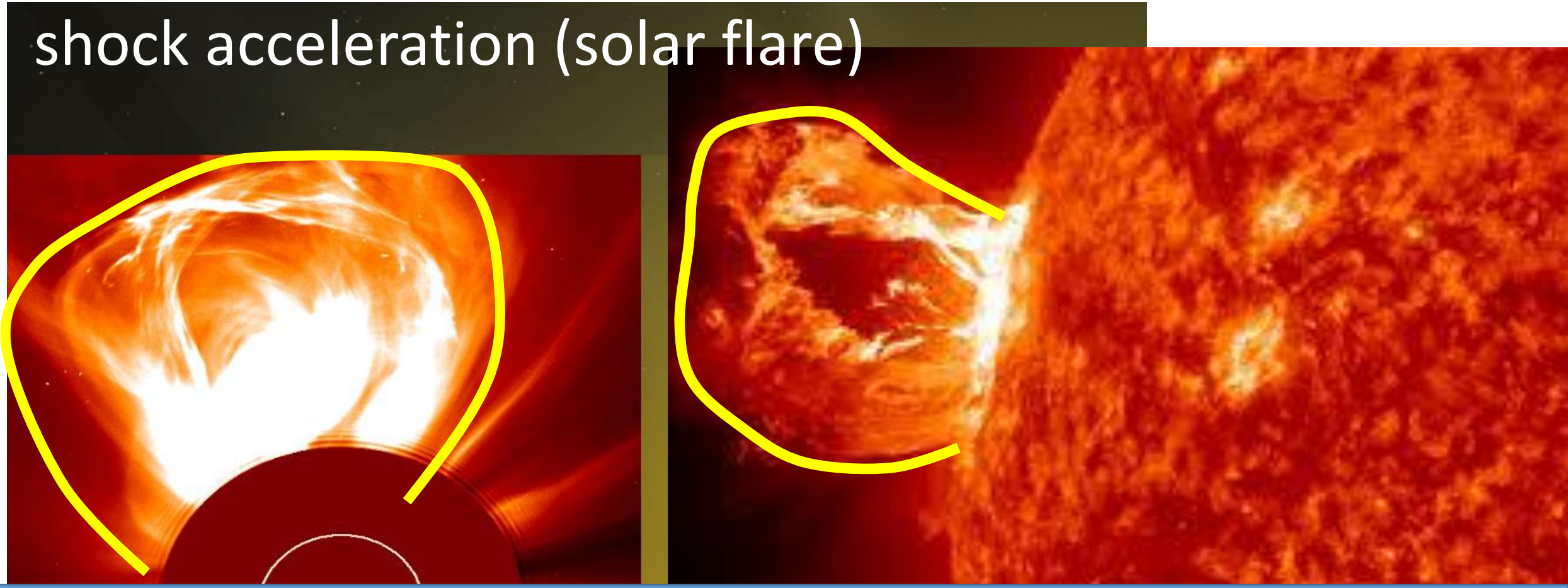

- **GLEs are sudden increases in the cosmic ray intensity. The historical beginning of cosmic ray flux observations started with the occurrence of GLE on 28 February 1942.**

- **Divided, controversially, into impulsive (acceleration in solar flare) and gradual events (acceleration in CME)?**

Helioclimatology

Cosmic ray spallation is suspected to be the cause of abundance of some light elements in the universe such as beryllium; through a process known as cosmogenic nucleosynthesis.

Also, other elements such as carbon-14 and chlorine are formed within the solar system via cosmic ray spallation. This is termed cosmogenic nuclides.

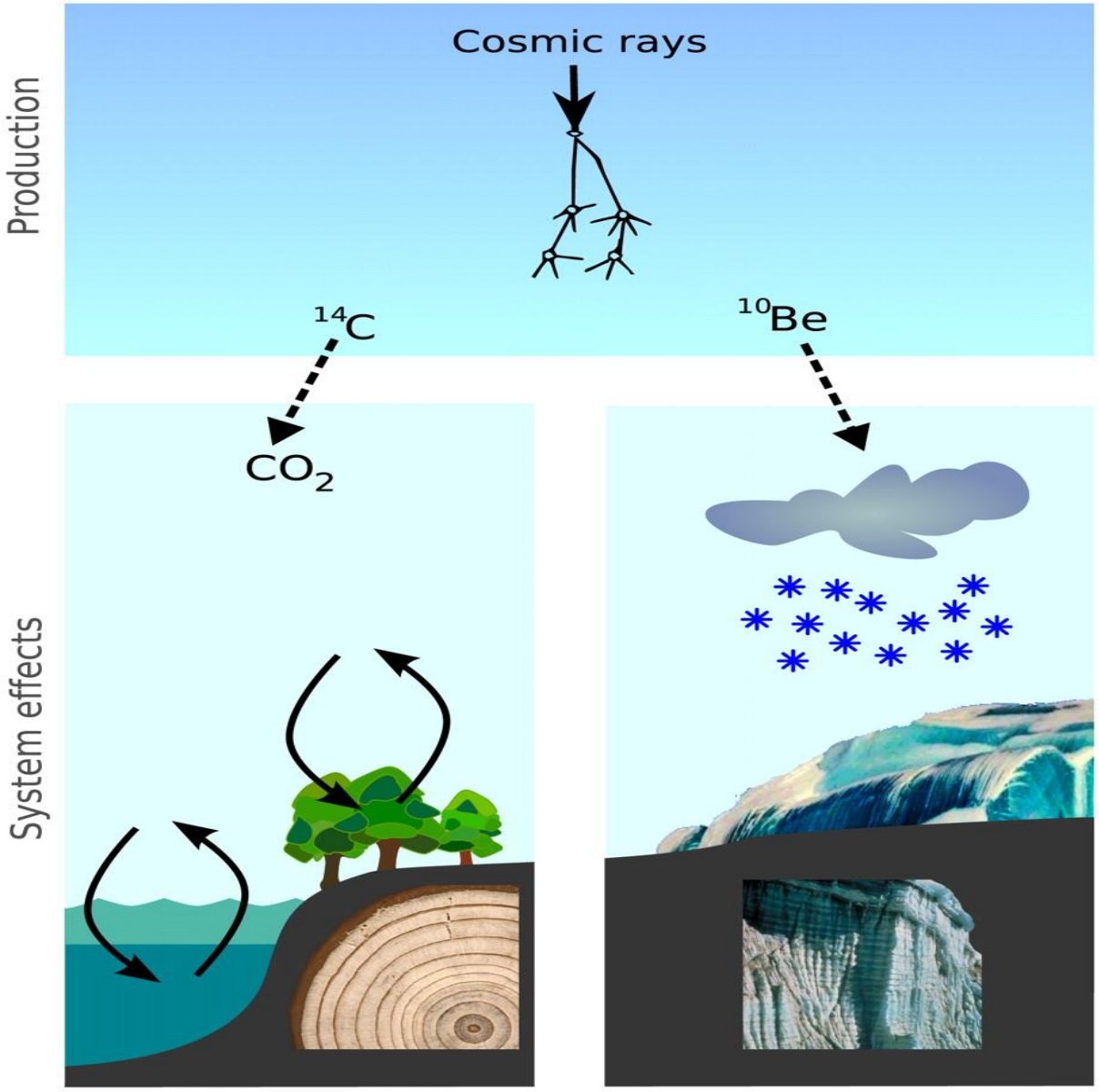

Ground-level Enhancement (GLE) = "cosmic" rays from sun

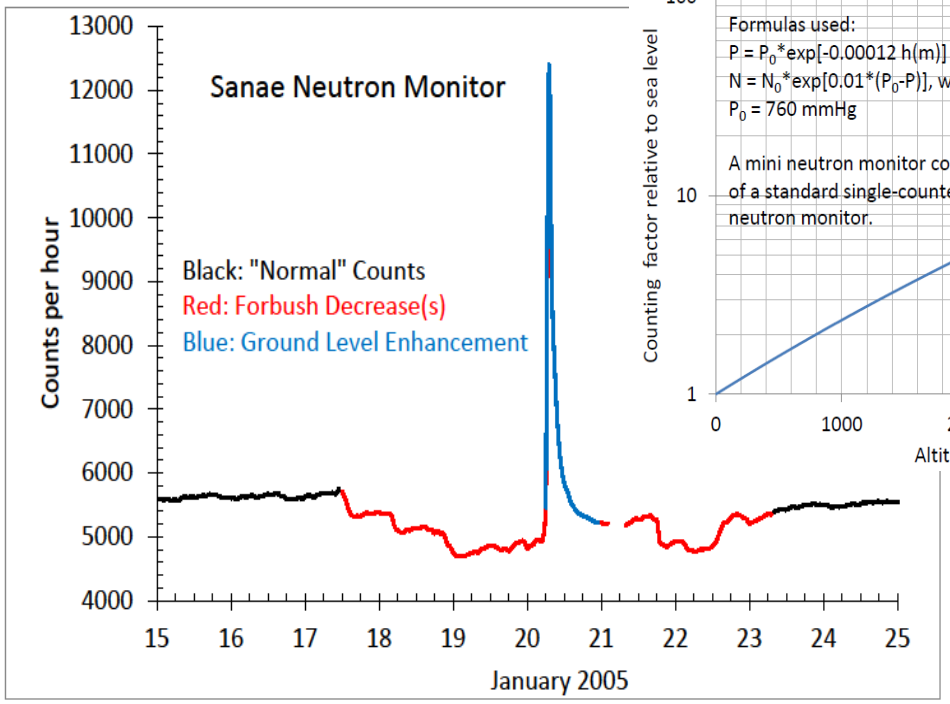

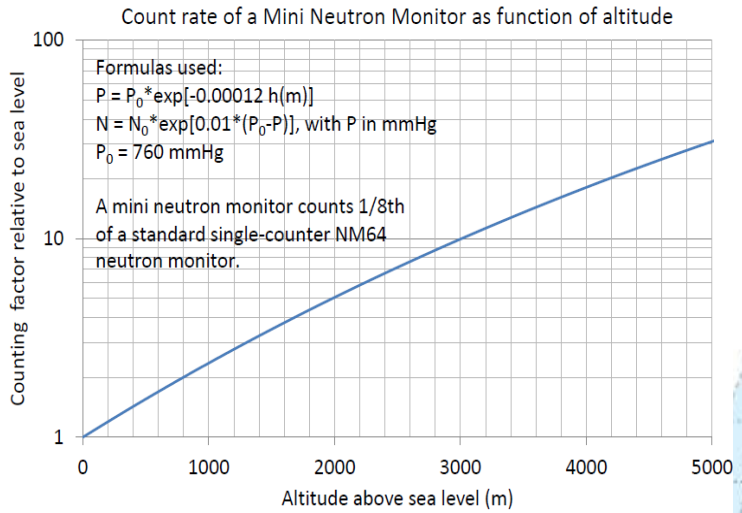

Sanae Neutron Monitor

Ground-level Enhancement (GLE) = "cosmic" rays from sun (space experiment)

The Earth's neutral monitor (NM) network has one important advantage above space experiments, which is sensitivity to arrival direction of particles. This gives indication of anisotropy of the event

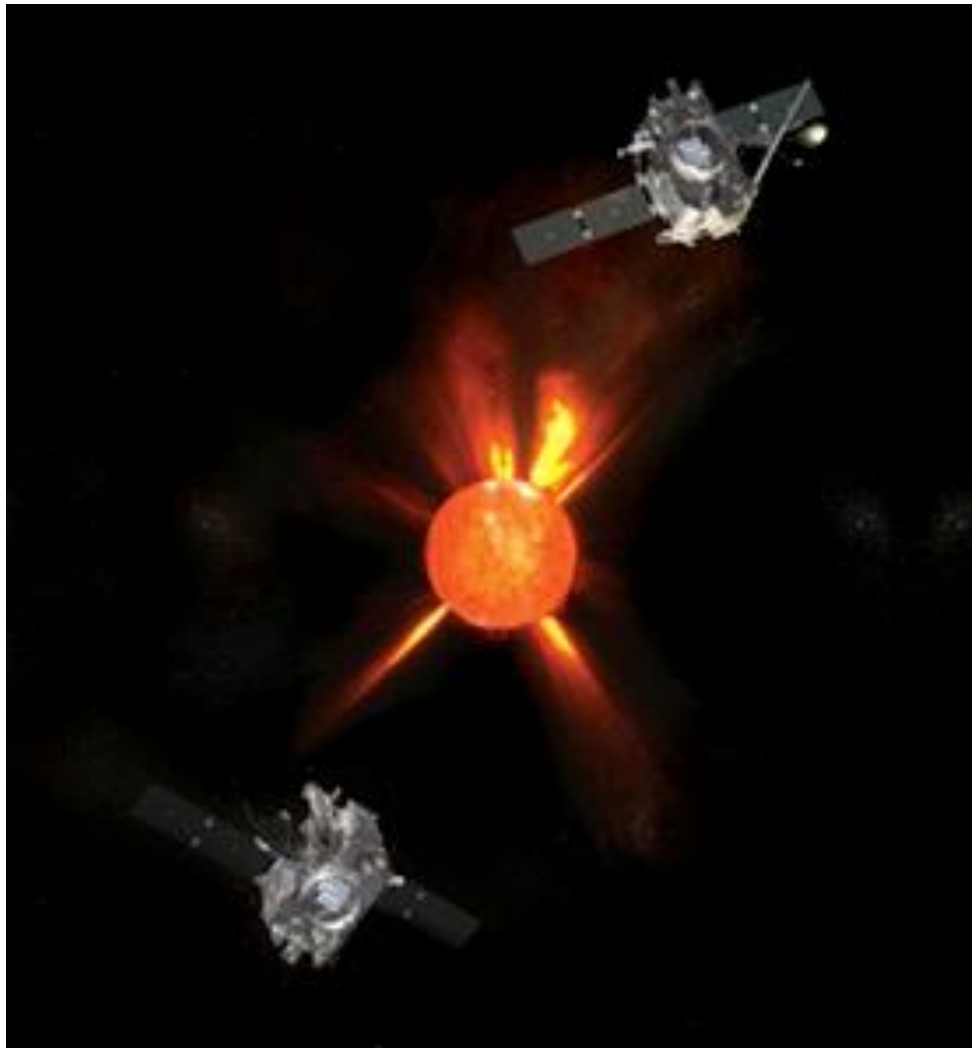

See:

- **Particles (GLE)**
- **Flare and CME (3D-stereo)**
- **Shock (3D-stereo)**
- **Gammas**
- **X-rays**
- **Radio**
- **Magnetic fields**
- **Kinks**

"A window into Geospace" (Poles are better)

The Window into Geospace…..

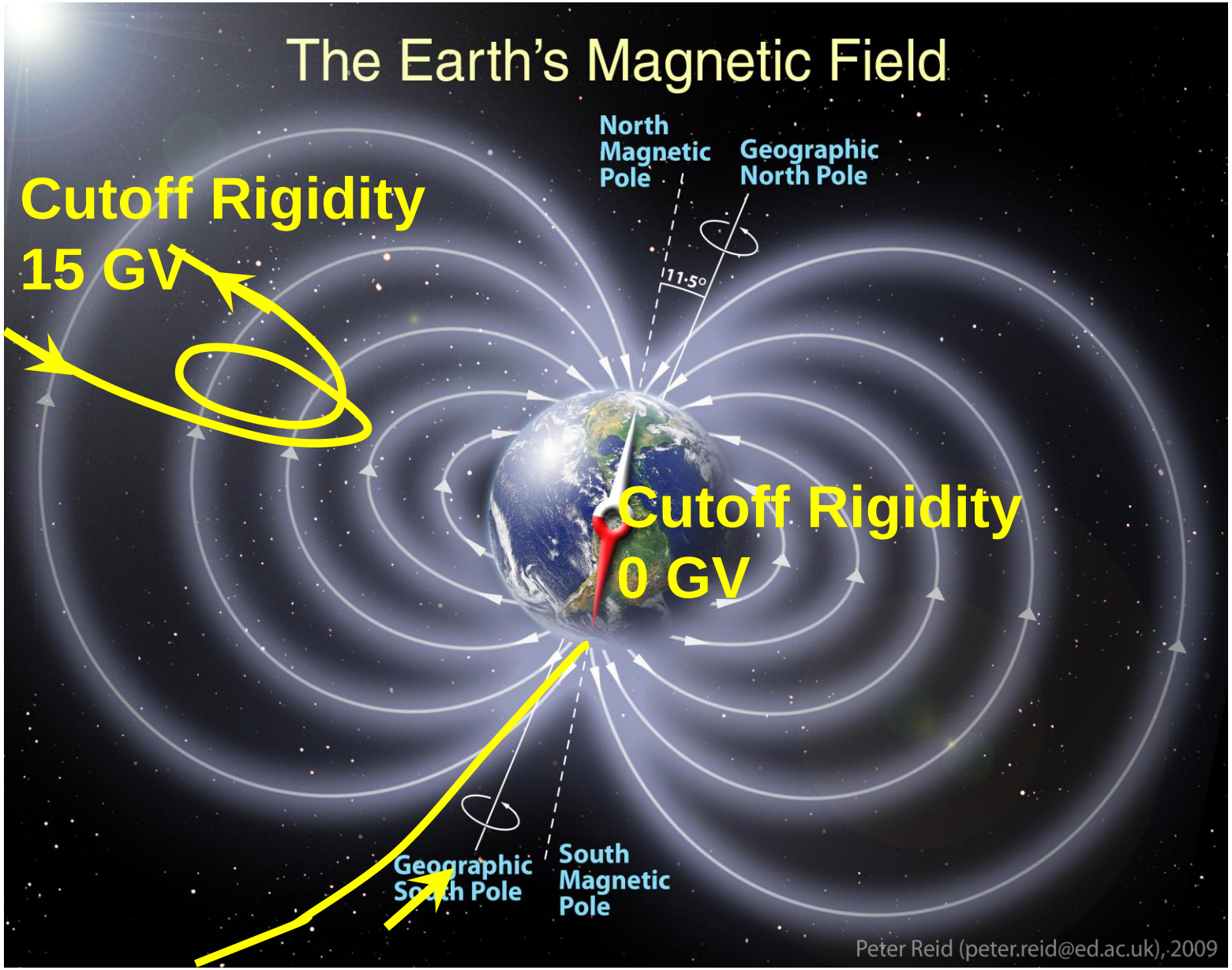

The Window into Geospace…..

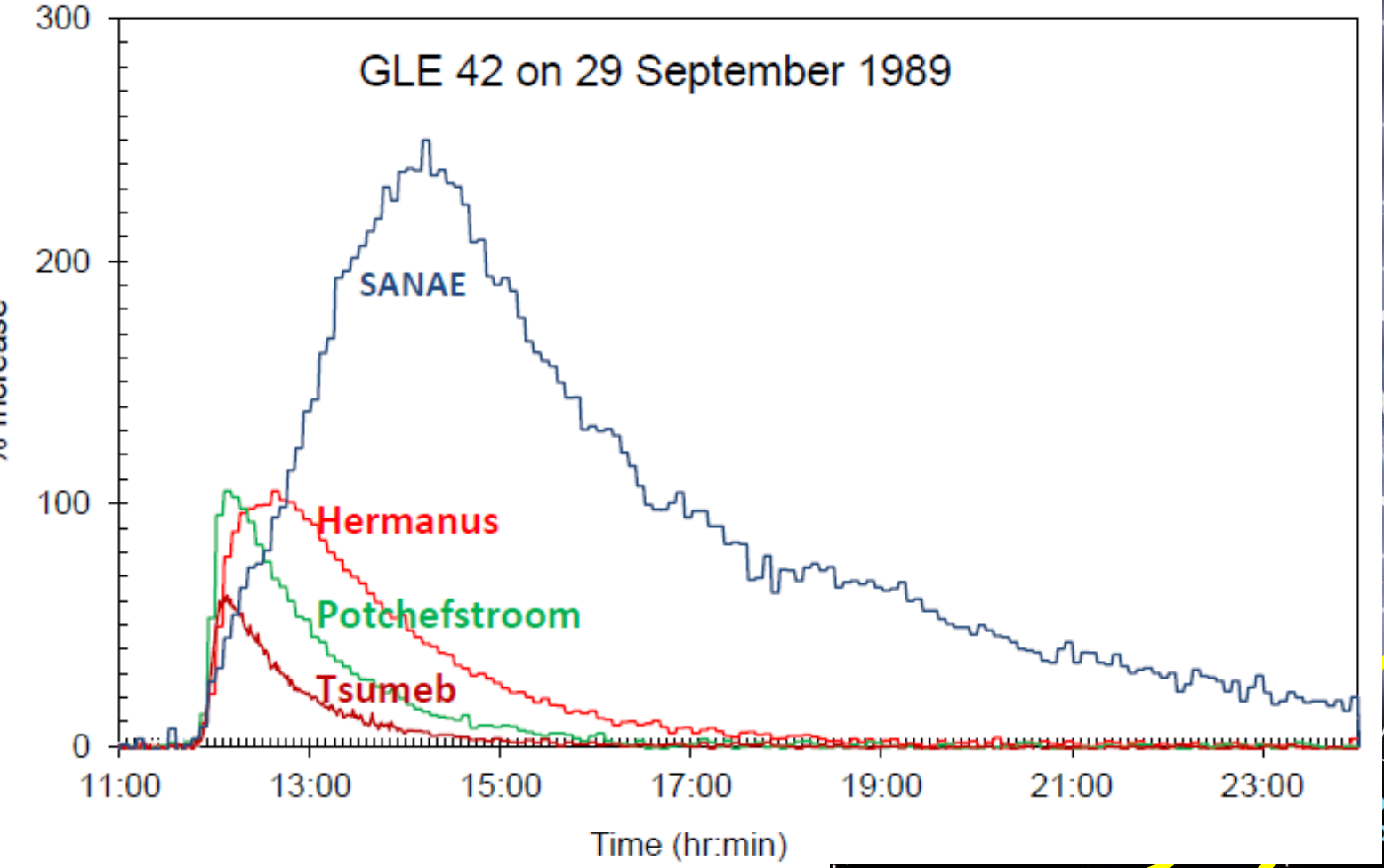

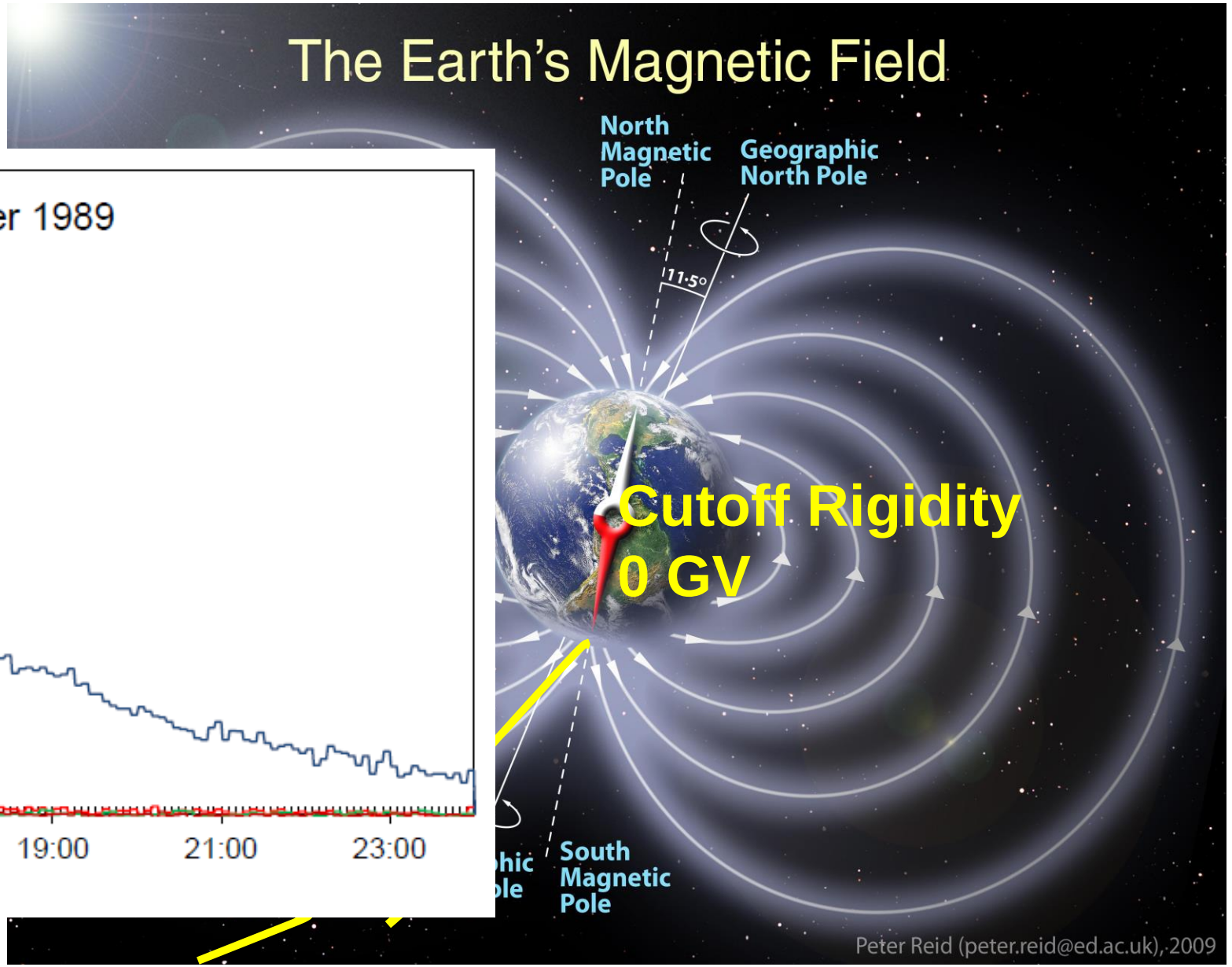

The best observed two GLEs

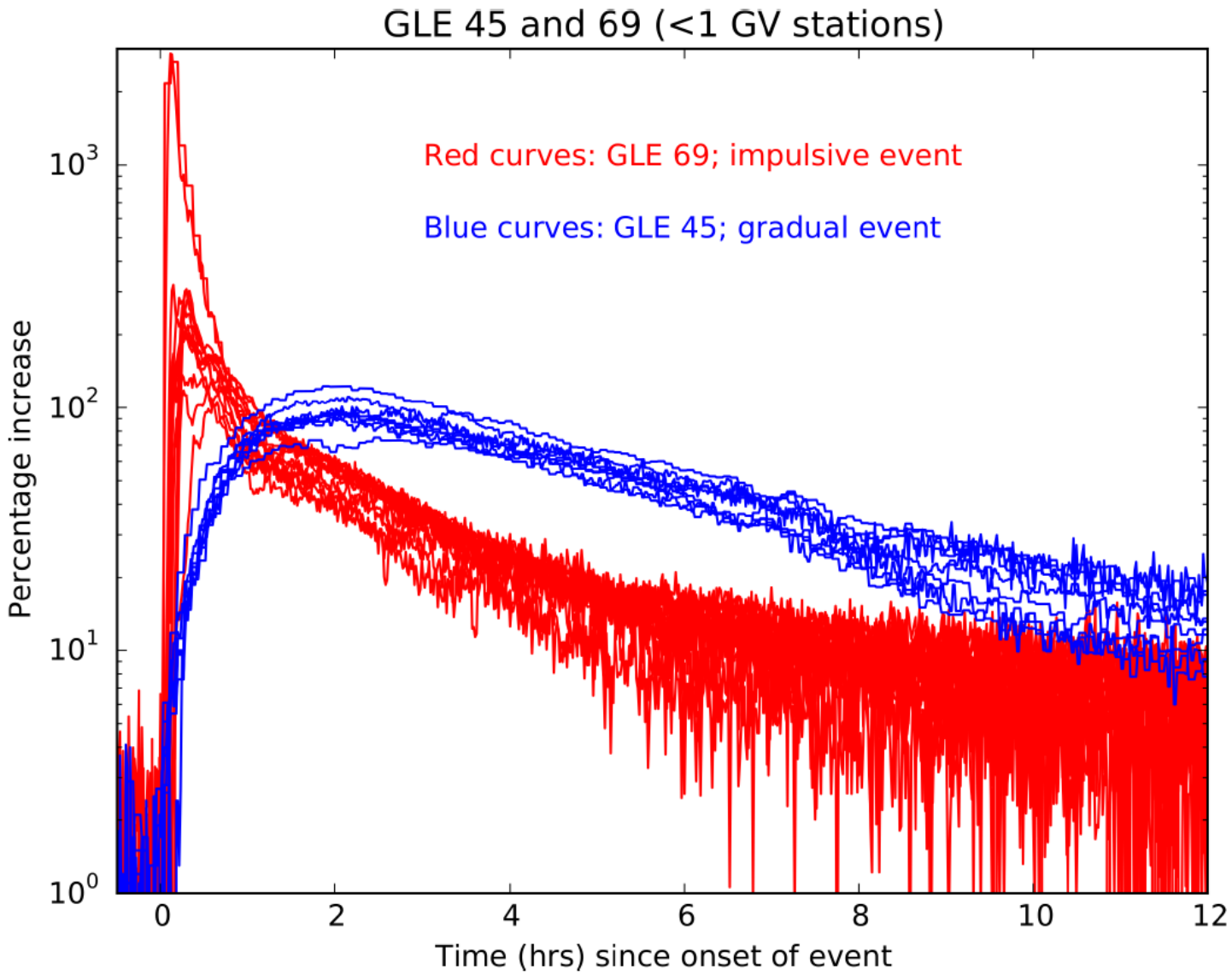

Is there any better explanation on the controversial classification based on more realistic physical interpretation?

Selected GLEs for this study

A summary of the GLE events selected for this study.

GLE no.	Sol. long.[a] (° W)	Max. increase[b] (%)	No. of NMs[c]	Rise time (min)	Decay time (min)
30	36	23	9	27.6	67.2
31	65	32	8	16.6	10.8
39	130	37	11	6.0	16.8
43	-20	45	10	94.8	413.4
45	51	88	10	82.8	226.2
48	60	12	9	6.0	81.0
51	60	10	10	40.2	148.8
52	70	24	10	33.0	57.0
60	15	84	12	1.2	3.0
63	-1	10	13	9.6	89.4
65	50	13	14	19.2	67.2
66	85	11	14	79.8	177.0
67	10	10	14	18.0	21.0
69	66	1056	13	3.0	4.8
70	25	422	12	1.8	6.0

[a]Ideal magnetic connection between the source of the SEPs and Earth would correspond to a source located at $\sim 60°$ W in terms of solar longitude.

The asymptotic cone of acceptance

GLE on 20 January 2005 (only < 1 GV NM stations)

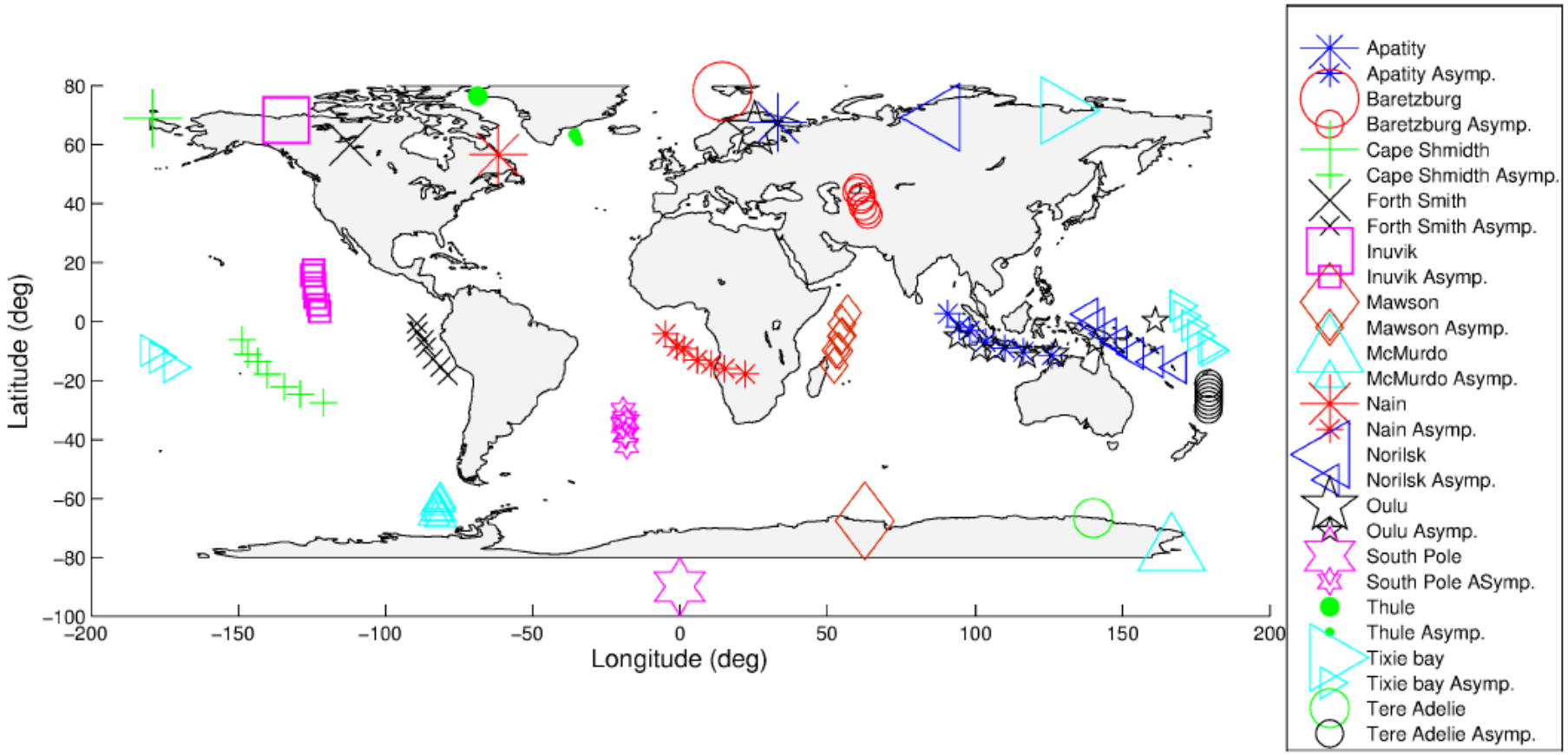

Figure 2. Geographical locations of the contributing NMs with geomagnetic cut-off rigidity below 1 GV (large markers) and the corresponding asymptotic viewing directions (small markers). For each NM, the asymptotic viewing direction was calculated for rigidities of 0.7, 1.4, 2.1, 2.9, 3.6, 4.3 and 5.0 GV, with the highest rigidity position closest to each station.

- **For vertical arrival at a neutron monitor, the particles must have come from a so-called asymptotic direction in space before they penetrated the geomagnetosphere.**

Are they magnetically connected to Earth?

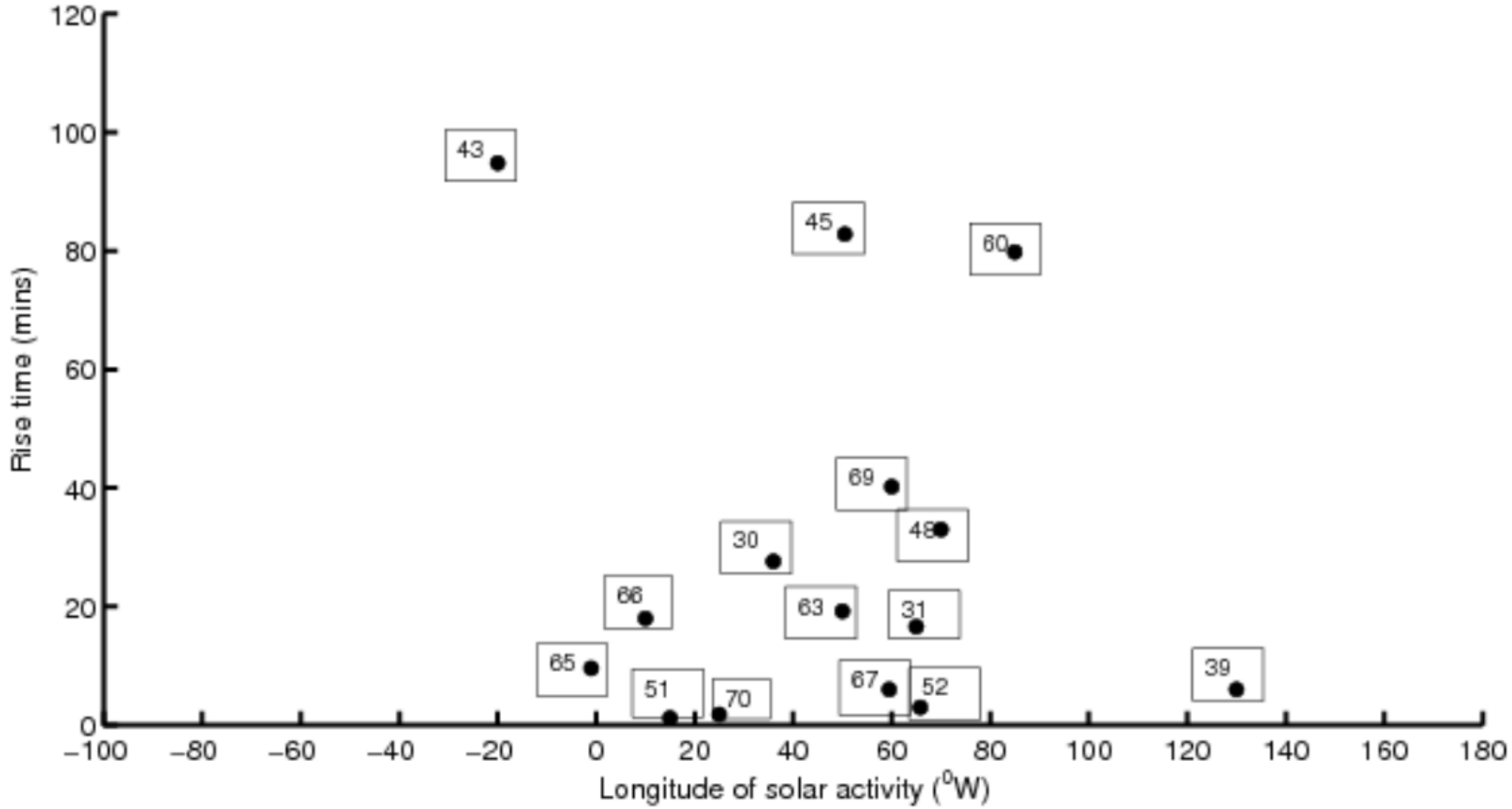

OMNI-DIRECTIONAL INTENSITY

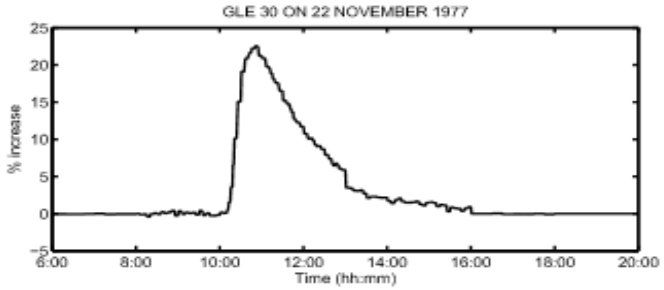

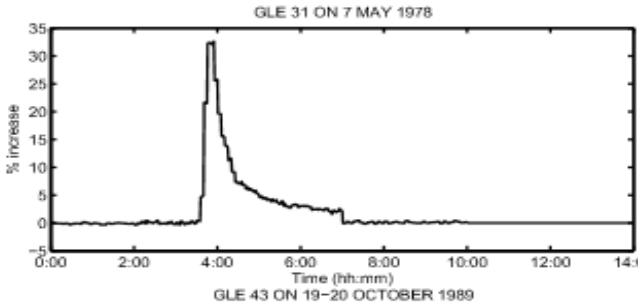

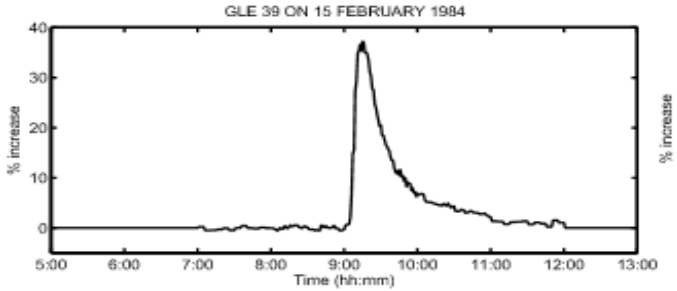

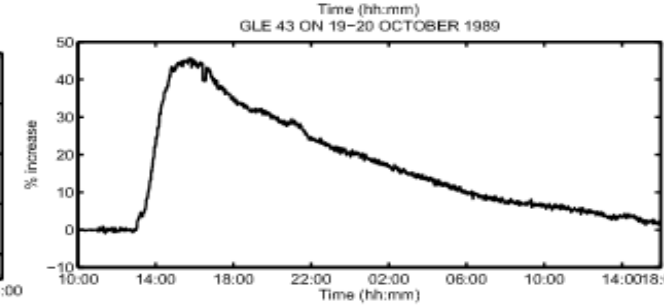

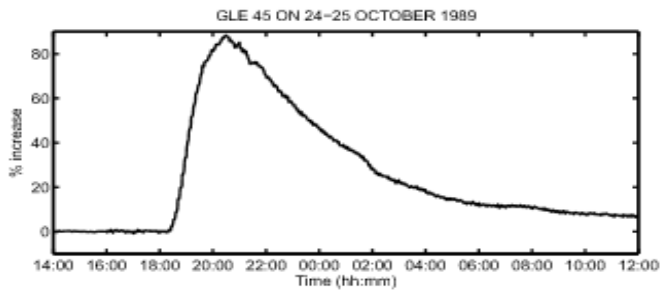

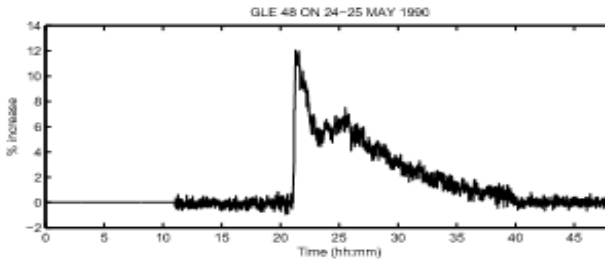

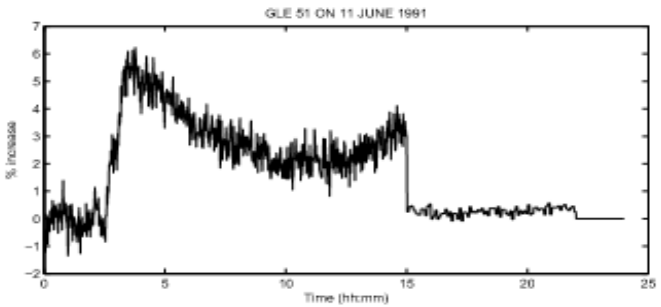

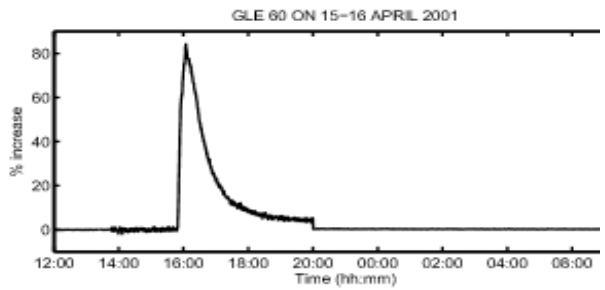

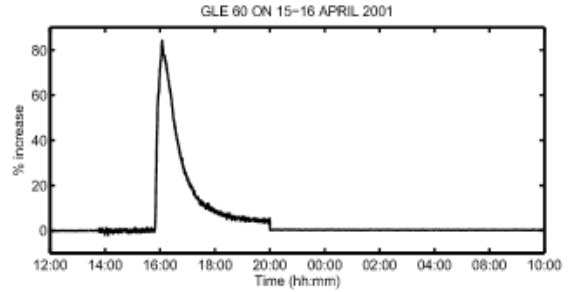

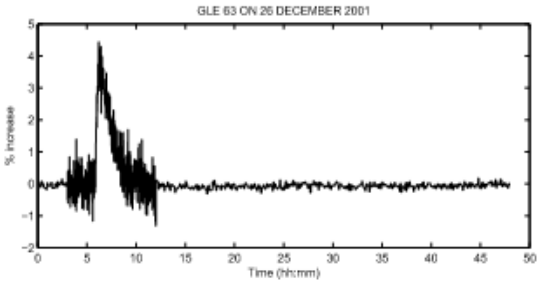

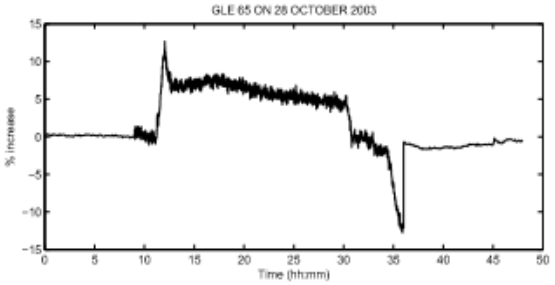

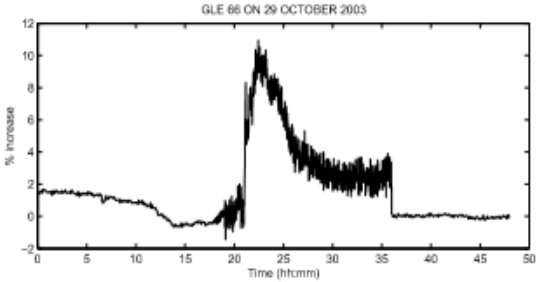

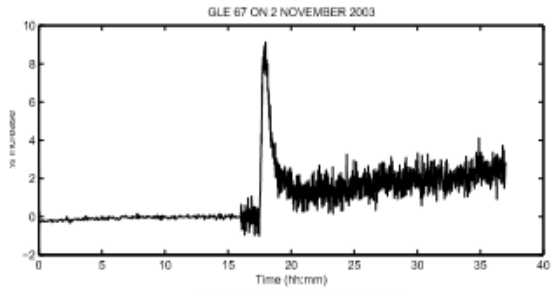

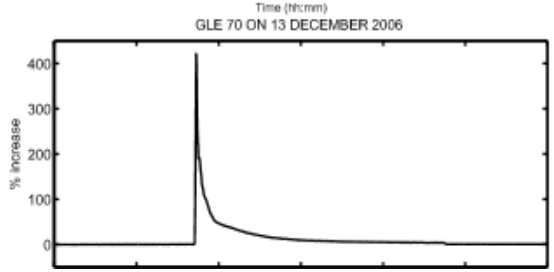

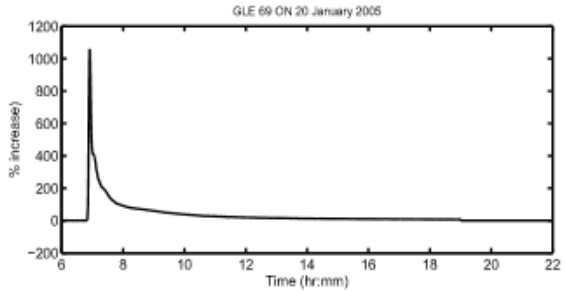

Rise time instead of time to the maximum

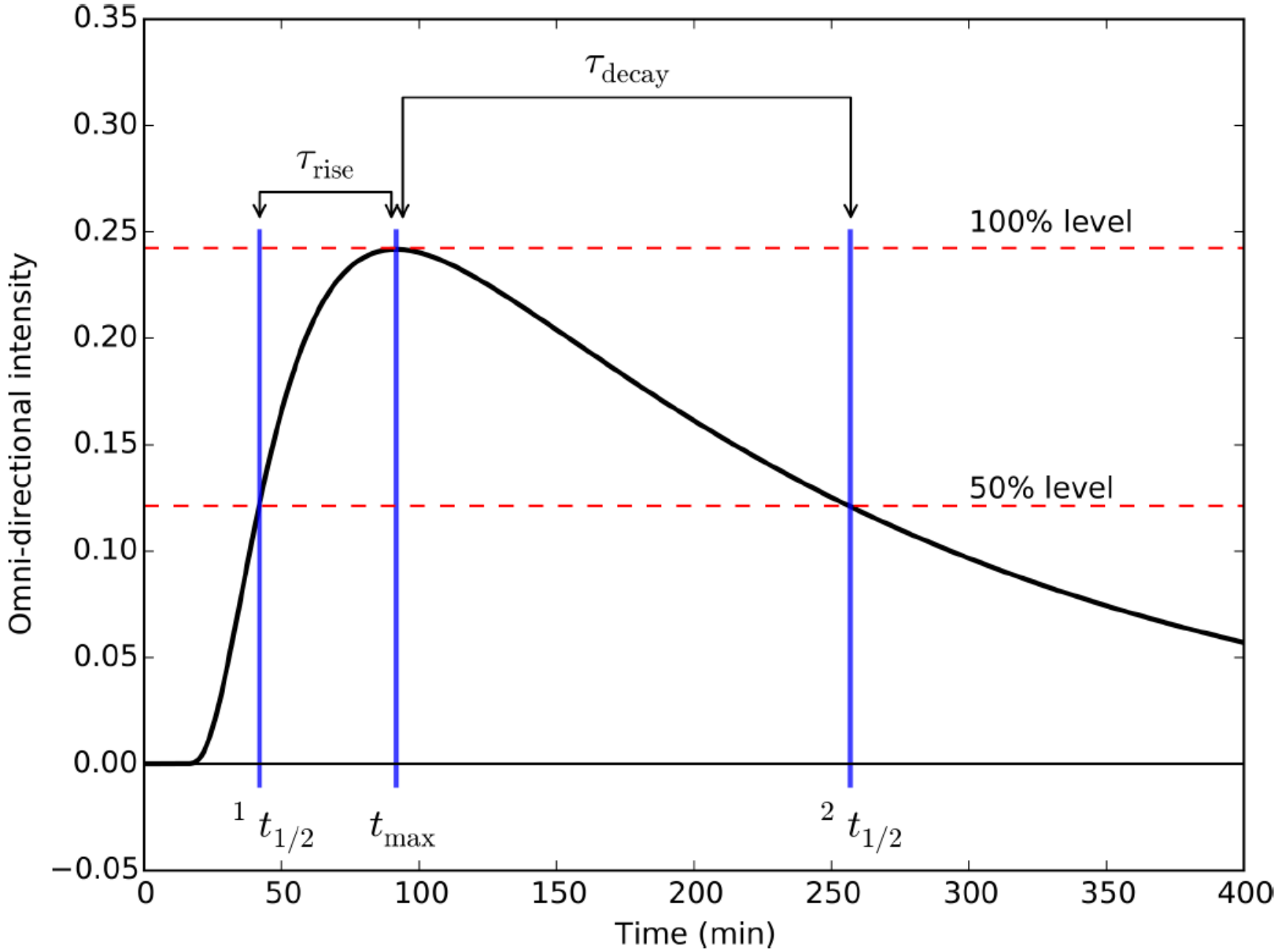

Illustrating how we characterize the pulse shape of a GLE through the rise and decay times.

Relationship between rise and decay time

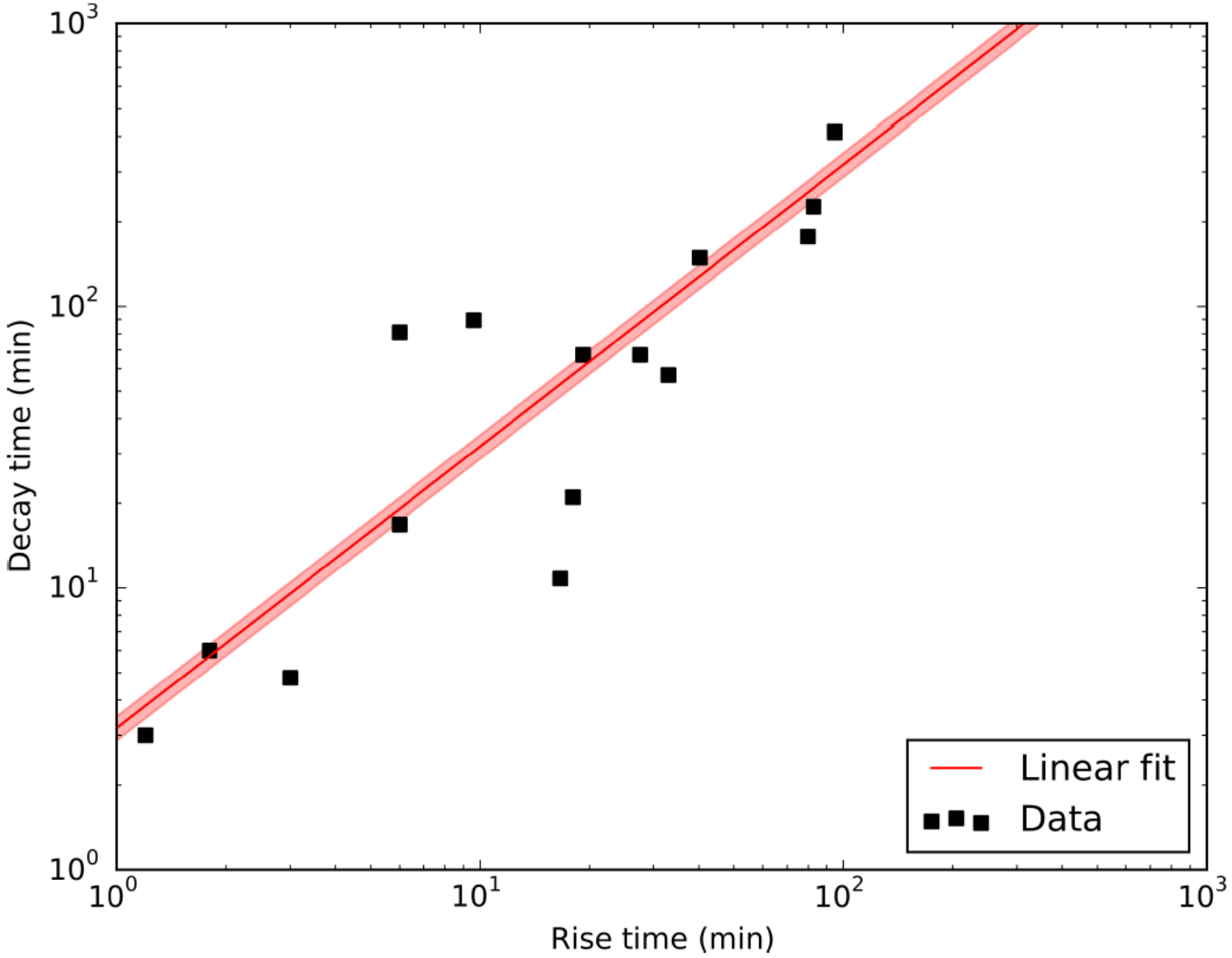

The data points show the rise and decay times as calculated for our selection of 15 GLEs. The red line shows a linear t to the observations, while the red band indicates a 1σ (standard deviation) error on the fitted slope.

Interpretation in terms of diffusive transport theorem.

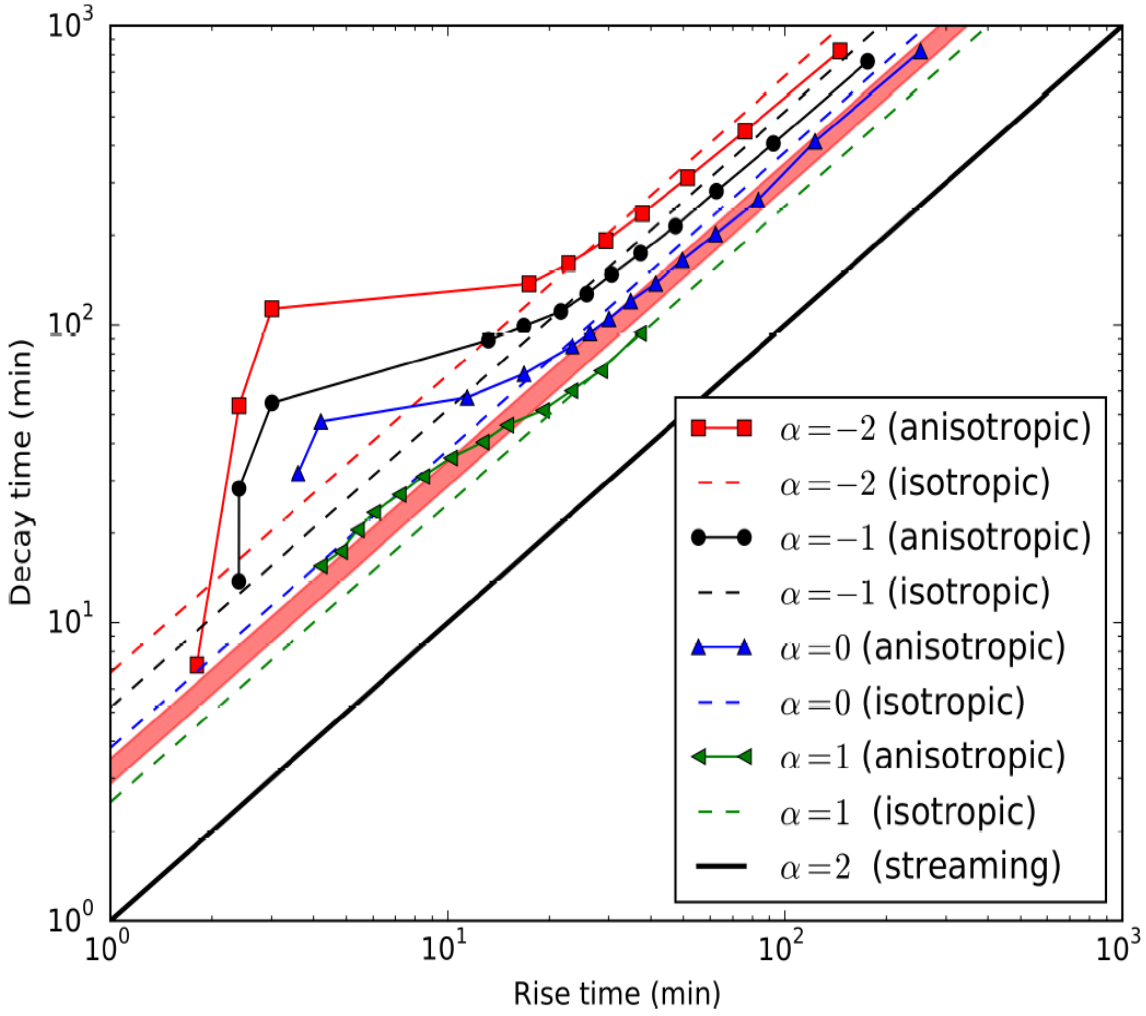

The symbols show the modelled relationship between r and d for different values of α, while the dashed lines are the corresponding analytical approximations.

$$\frac{\partial f}{\partial t} = \frac{1}{r^2}\frac{\partial}{\partial r}\left[r^2 \kappa \frac{\partial f}{\partial r}\right].$$

If the diffusion coefficient is of the form κ=κ0(r/r0)α, the solution for an impulsive injection at t = 0 and r = 0

$$f \propto t^{3/(\alpha-2)} \exp\left[\frac{-r^2 (r_0/r)^{\alpha}}{(2-\alpha)^2 \kappa_0 t}\right].$$

We call this the point-diffusion solution.

$$\frac{t_{1/2}}{t_p} = 2^{\frac{2-\alpha}{3}} \exp\left(1 - \frac{t_p}{t_{1/2}}\right).$$

This has two solutions, for $t < t_p$ and $t > t_p$. They are the rise and decay times to half the maximum intensity. It is noteworthy that this ratio is independent of the radial distance, r, and the magnitude of the diffusion coefficient, κ. It only depends on the radial dependence of κ. For α = 0, 1, and 2, corresponding to $\kappa \propto r^0$, $\kappa \propto r$ and $\kappa \propto r^2$, the solution of (5) is $t_{1/2}/t_p$ = 3.13; 2.15; and 1.07 respectively. These values can conveniently be parameterized as $t_{1/2}/t_p \approx 3 - \alpha$.

REST IN PEACE

Using Strauss-modified numerical transport model

Strauss and Fichtner, 2015 for details.

$$\boldsymbol{B}(r,\theta) = \frac{B_0 r_0^2}{r^2}(\hat{r} - \tan\Psi\hat{\phi}),$$

$$\frac{\partial f}{\partial t} + \overbrace{\frac{1}{r^2}\frac{\partial}{\partial r}(\mu v \cos\Psi(r^2 f)) + \frac{\partial}{\partial \phi}\left(-\frac{\mu v \sin\Psi}{r} f\right)}^{\text{focusing}}$$

$$+ \overbrace{\frac{\partial}{\partial \mu}\left(\frac{1-\mu^2}{2L} v f\right)}$$

$$= \overbrace{\frac{1}{r^2}(r^2 D_\perp^{(rr)})\frac{\partial f}{\partial r} + \frac{D_\perp^{(r\phi)}}{r}\frac{\partial^2 f}{\partial r \partial \phi} + D_\perp^{(rr)}\frac{\partial^2 f}{\partial r^2}}^{\text{diffusion in } r}$$

$$+ \overbrace{\frac{\partial}{\partial \mu}\left(D_{\mu\mu}\frac{\partial f}{\partial \mu}\right)}^{\text{diffusion in } \mu}$$

$$+ \overbrace{\frac{1}{r^2}\frac{\partial}{\partial r}(r D_\perp^{(\phi r)})\frac{\partial f}{\partial \phi} + \frac{D_\perp^{(\phi r)}}{r}\frac{\partial^2 f}{\partial r \partial \phi} + \frac{D_\perp^{(\phi\phi)}}{r^2}\frac{\partial^2 f}{\partial \phi^2}}^{\text{diffusion in } \phi},$$

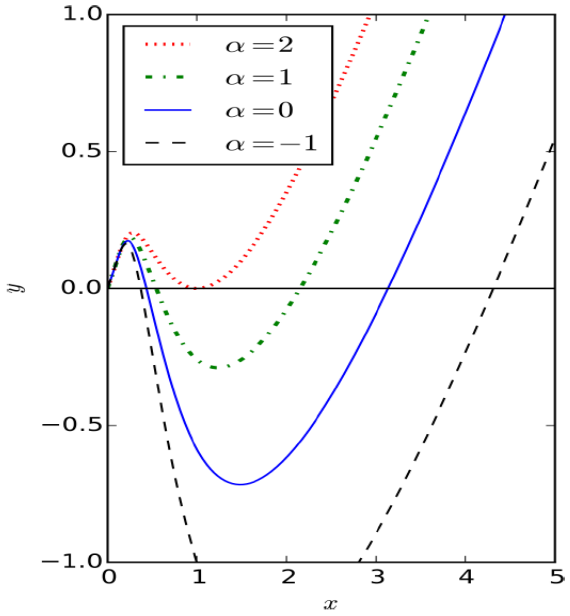

Finding the roots of Equation for different values of α.

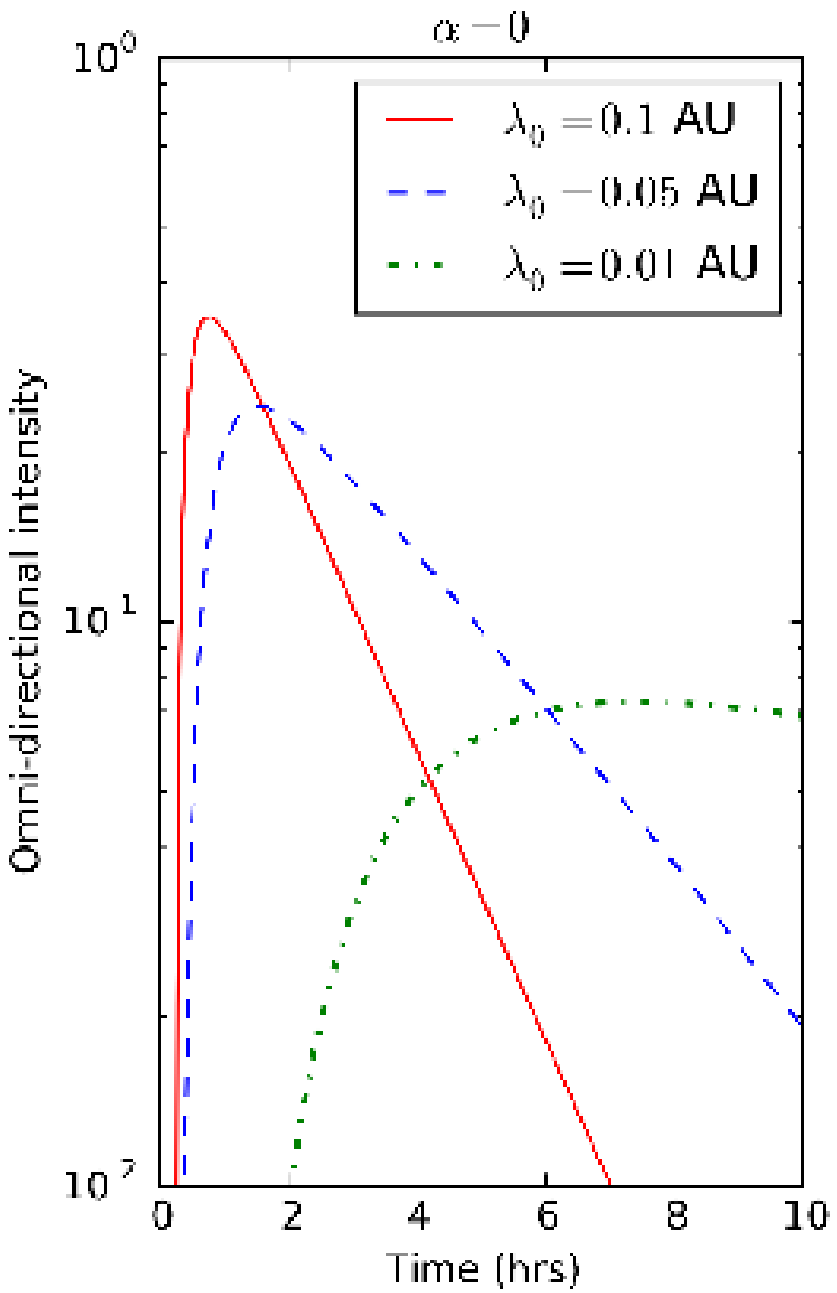

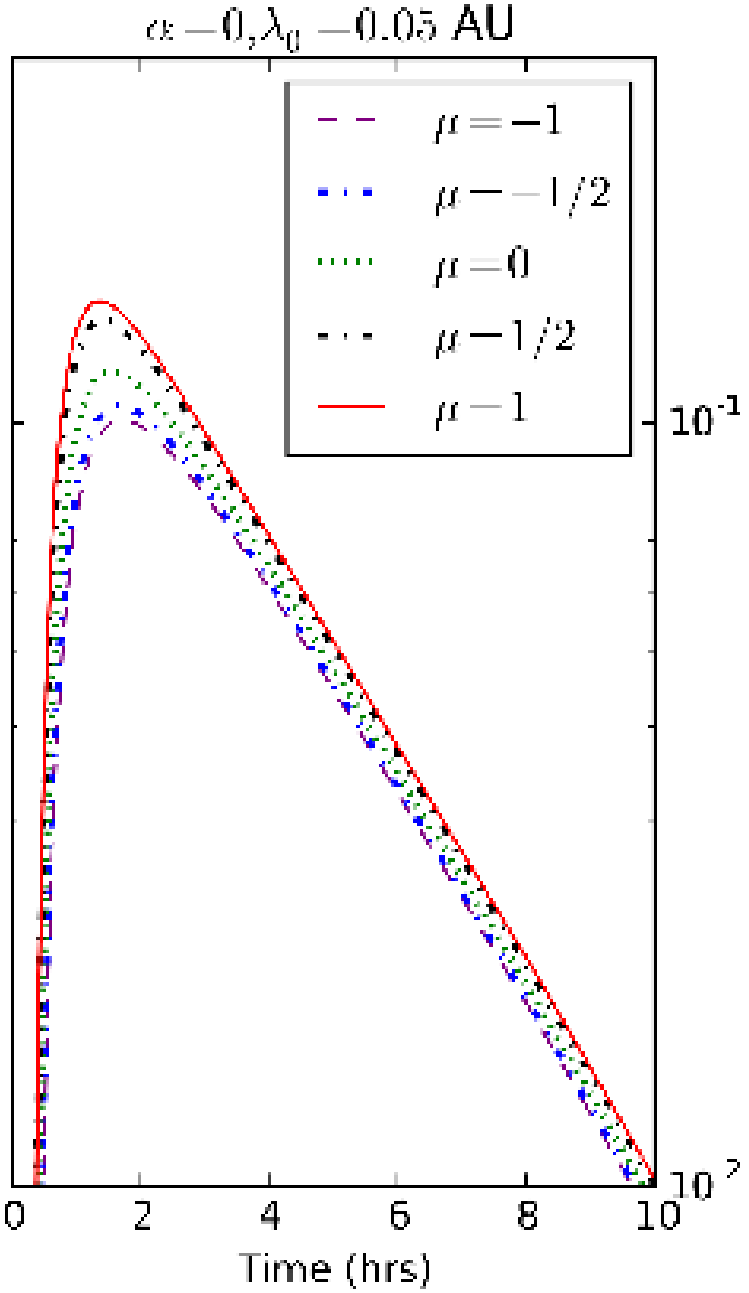

Results

Salient features

By calculating the rise and decay times for a subset of all GLE events, we find a linear relationship between these two quantities, conveniently summarized as $\tau_d \sim 3\tau_r$, i.e. the decay phase lasts, on average, 3 times longer than the rising phase of the event.

This relationship seems to hold for a large range of τ_d and τ_r values (at least two orders of magnitude), suggesting that GLEs do not fall into two distinct classes of either impulsive or gradual events, but follows a continuous distribution of impulsive-like or gradual-like events. It is difficult to

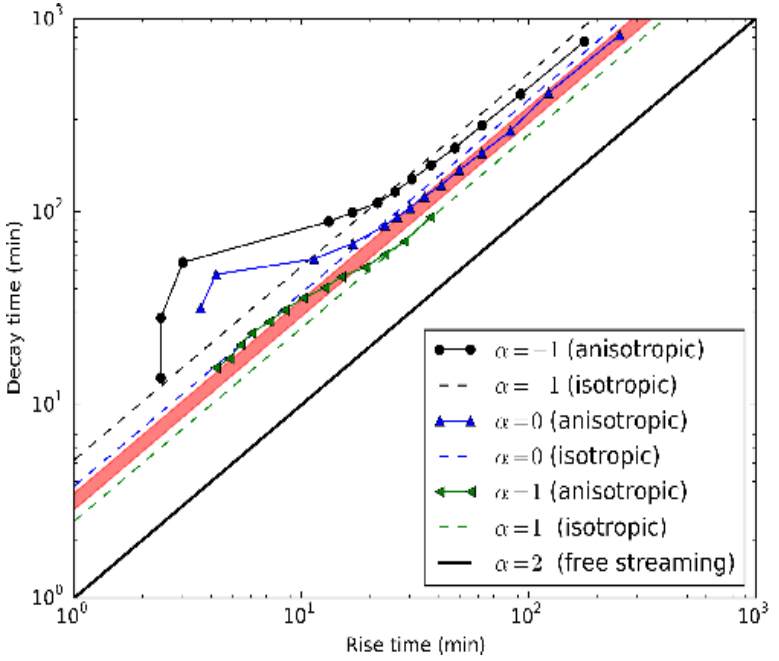

It is difficult to imagine how different acceleration mechanisms can lead to such a "universal" (in the sense that it is the same for events historically characterized as either impulsive or gradual) linear relationship, and hence we interpret this result in terms of an interplanetary transport model.

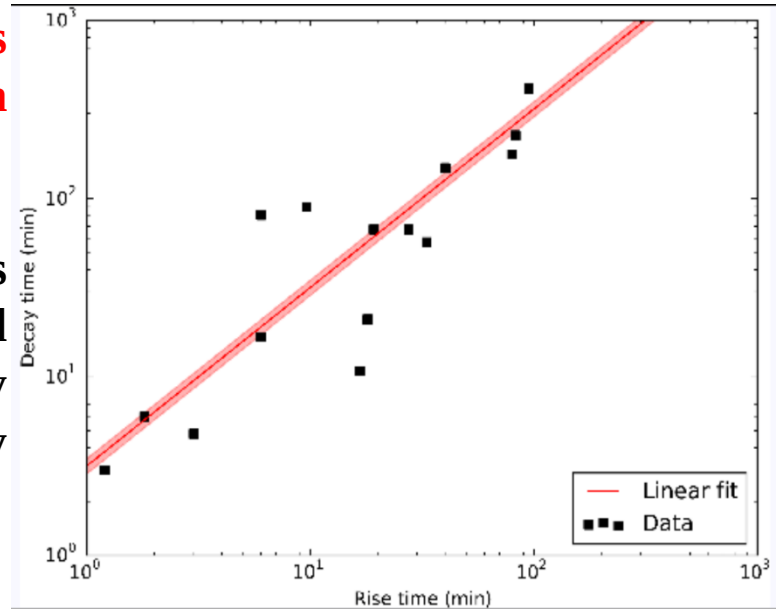

In the limit of very effective particle scattering, i.e. when the resulting distribution is nearly isotropic, both the numerical and analytical solutions reproduce the observed linear trend. We thus conclude that interplanetary transport may have an extremely large effect on the observed pulse shape of GLEs and should not be completely ignored as is mostly done.

Acknowledgements

Prof. Harm Moraal, Prof. Pieter Stoker, Dr. Du Toit Strauss, Helena Krüger, Anne Mans, Gert Benadé + Students + cosmic-ray and astrophysics working group
+ Antarctic expedition members of North-West University, Potchefstroom

They have been funded by

- **the NRF and its predecessors, and**
- **the South African National Antarctic Programme**

Thank you!

Appendix?

The standard Parker HMF is given by

$$\boldsymbol{B}(r,\theta) = \frac{B_0 r_0^2}{r^2}(\hat{r} - \tan\Psi\hat{\phi}), \tag{A1}$$

where B_0 is some reference value at r_0. The magnitude of the HMF, however, never enters any calculations here, and only the geometry is of importance. The HMF spiral angle (Ψ, the angle between the HMF and the radial direction) is defined by

$$\tan\Psi = \frac{\Omega r \sin\theta}{V_{\rm sw}}, \tag{A2}$$

with Ω being the angular rotation speed of the Sun and being $V_{\rm sw} = 400\,{\rm km\,s^{-1}}$ the solar wind speed. As the model is limited to the ecliptic regions of the heliosphere, $\sin\theta = 1$ is assumed throughout. Moreover, since the Parker HMF is independent of ϕ, all transport quantities are also assumed to be independent.

With this definition,

$$\hat{b} = \cos\Psi\hat{r} - \sin\Psi\hat{\phi}, \tag{A3}$$

which determines the streaming direction in Equation (1), while the diffusion tensor takes the form (see also the discussion by Effenberger et al. 2012)

$$\begin{aligned}\mathbf{D}_\perp &= \begin{pmatrix} D_\perp^{(rr)} & D_\perp^{(r\phi)} \\ D_\perp^{(\phi r)} & D_\perp^{(\phi\phi)} \end{pmatrix} \\ &= \begin{pmatrix} D_\perp \sin^2\Psi & D_\perp \sin\Psi\cos\Psi \\ D_\perp \sin\Psi\cos\Psi & D_\perp \cos^2\Psi \end{pmatrix},\end{aligned} \tag{A4}$$

where $D_\perp$ is the perpendicular diffusion coefficient specified in the local HMF aligned coordinate system. Also note that $D_\perp^{(\phi r)} = D_\perp^{(r\phi)}$. As an illustration, the values of $\cos\Psi$, $\sin\Psi$, and $\cos\Psi\sin\Psi$ are shown in Figure 10 as a function of radial distance.

The TPE in spherical coordinates then becomes

$$\begin{aligned}\frac{\partial f}{\partial t} &+ \overbrace{\frac{1}{r^2}\frac{\partial}{\partial r}(\mu v \cos\Psi(r^2 f))}^{\text{streaming in } r} + \overbrace{\frac{\partial}{\partial\phi}\left(-\frac{\mu v \sin\Psi}{r} f\right)}^{\text{streaming in } \phi} \\ &+ \overbrace{\frac{\partial}{\partial\mu}\left(\frac{1-\mu^2}{2L} v f\right)}^{\text{focusing}}\end{aligned} \tag{A5}$$

$$\begin{aligned}&= \overbrace{\frac{1}{r^2}\left(r^2 D_\perp^{(rr)}\right)\frac{\partial f}{\partial r} + \frac{D_\perp^{(r\phi)}}{r}\frac{\partial^2 f}{\partial r\partial\phi} + D_\perp^{(rr)}\frac{\partial^2 f}{\partial r^2}}^{\text{diffusion in } r} \\ &+ \overbrace{\frac{\partial}{\partial\mu}\left(D_{\mu\mu}\frac{\partial f}{\partial\mu}\right)}^{\text{diffusion in } \mu}\end{aligned} \tag{A6}$$

$$+ \overbrace{\frac{1}{r^2}\frac{\partial}{\partial r}\left(r D_\perp^{(\phi r)}\right)\frac{\partial f}{\partial\phi} + \frac{D_\perp^{(\phi r)}}{r}\frac{\partial^2 f}{\partial r\partial\phi} + \frac{D_\perp^{(\phi\phi)}}{r^2}\frac{\partial^2 f}{\partial\phi^2}}^{\text{diffusion in } \phi}, \tag{A7}$$

which is the equation to be solved by applying a suitable numerical scheme.

A numerical solution of the equation above requires some careful consideration. If the advection terms (streaming and